Detection and Characterization of Uranium-Humic Complexes During 1D Transport Studies

Emily K. Lesher[1,*], Bruce D. Honeyman[1], James F. Ranville[2]

Abstract

The speciation and transport through porous media of uranium (VI) is highly dependent on solution conditions, the presence of complexing ligands, and the nature of the porous media. The dependency on many variables makes prediction of U transport in bench-scale experiments and in the field difficult. In particular, the identification of colloidal U phases poses a technical challenge.

Transport of U in the presence and absence of natural organic matter (Suwannee River humic acid, SRHA) through silica sand and hematite coated silica sand was tested at pH 4 and 5 using static columns, where flow is controlled by gravity and residence time between advective pore volume exchanges can be strictly controlled. The column effluents were characterized by traditional techniques including total [U], total [Fe], [DOC], and pH analysis, and also by non-traditional techniques: field flow fractionation with online ICP-MS detection (FFF-ICP-MS) and specific UV absorbance (SUVA) characterization of effluent fractions.

Key results include that the transport of U through the columns was enhanced by pre-equilibration with SRHA, and previously deposited U was remobilized by the addition of SRHA. The advanced techniques yielded important insights on the mechanisms of transport: FFF-ICP-MS identified a U-SRHA complex as the mobile U species and directly quantified relative amounts of the complex, while specific UV absorbance (SUVA) measurements indicated a composition-based fractionation onto the porous media.

Keywords: uranium, humic substances, transport, field-flow fractionation, FFF-ICP-MS, SUVA

*Corresponding author
Email address: emily.lesher@gmail.com (Emily K. Lesher)
[1]Colorado School of Mines, Civil and Environmental Engineering, Golden, Colorado, USA
[2]Colorado School of Mines, Department of Chemistry and Geochemistry, Golden, Colorado, USA

Detection and Characterization of Uranium-Humic Complexes During 1D Transport Studies

Emily K. Lesher[1,*], Bruce D. Honeyman[1], James F. Ranville[2]

1. Introduction

Nuclear power provided 69% of the non-carbon-based electricity (21% of total electricity) in the United States in 2010 (Kazimi et al., 2010, EIA, 2011). It will likely continue to be a significant part of the world's power portfolio for the near future as the market for low and no carbon energy sources thrives. The nuclear fuel cycle presents a number of potential points where uranium (U) can enter the environment: mining (*in situ* recovery or open pit), milling, conversion and enrichment (which also results in 10 to 20 times as much byproduct depleted uranium as fuel), use, storage of spent nuclear fuel, and waste disposal (Kazimi et al., 2010). The existence of federal programs (the Uranium Mill Tailings Remedial Action, UMTRA) addressing U contamination resulting from open pit mining and milling points to the likelihood of such excursions during the fuel cycle. Moreover, examples abound of naturally high concentrations of U in groundwaters (Prat et al., 2009, Ranville et al., 2007).

Modeling U transport and risk, understanding bioavailability and toxicity, and designing appropriate remediation or mitigation strategies requires a fundamental understanding of U behavior. The speciation of U in the hydrosphere is influenced by water chemistry parameters and the identity and concentrations of complexing ligands and surfaces. Sorption to surfaces or organic matter may change the mobility of U and its susceptibility to chemical or biological techniques intended to immobilize U *in situ*.

*Corresponding author
Email address: emily.lesher@gmail.com (Emily K. Lesher)
[1]Colorado School of Mines, Civil and Environmental Engineering, Golden, Colorado, USA
[2]Colorado School of Mines, Department of Chemistry and Geochemistry, Golden, Colorado, USA

In an open system, U(VI) speciation is dominated by the uranyl cation (UO_2^{2+}) at low pH, uranyl hydroxy complexes at neutral pH, and uranyl carbonato complexes at pH greater than 7. In a system with natural organic matter (NOM) and U(VI), U-NOM complexes are likely to form to an extent dependent on solution conditions including pH, Eh, and concentrations of ligand, U(VI), carbonate, and competing cations such as calcium (Moulin and Moulin, 1995, Moulin, 2005). U(VI) forms surface complexes with a variety of minerals including the metal oxides. The affinity of U(VI) for sites on an iron oxide surface can lead to the domination of metal speciation by the surface complex even when the iron oxide phase is a trace component in an aquifer matrix of mixed mineralogy (Davis et al., 1998) or is present as low concentration suspended particulates in a surface water. Silicon dioxide (quartz, silica) has a lower affinity for binding U(VI), but is a major aquifer constituent. Also commonly observed are ternary surface complexes that form between the metal oxide surface, a ligand (such as NOM), and U(VI).

The outcomes resulting from interactions among mineral surfaces, NOM, and metal ions are sometimes conflicting. NOM can adsorb onto mineral particles, and then through metal-ligand complexes retard transport through the porous media (Zachara et al., 1994) (Murphy and Zachara, 1995). This has even been proposed as a way to sequester contaminant metals in the subsurface (Nachtegaal and Sparks, 2003). In contrast, a metal-NOM solution complex may be more stable in solution than the metal ion alone, less prone to loss via adsorption, thus increasing metal mobility. These interactions, reactions, and their effects are highly dependent on pH, the mineral surface in question, the concentration and type of NOM present, kinetics, and the strength of the possible binary and ternary complexes, thus sweeping generalizations are very difficult (Murphy et al., 1999, Nachtegaal and Sparks, 2003).

Previous column studies have found enhanced U mobility through silica sand in the presence of NOM (fulvic acid (Tinnacher, 2008), humic acid (Mibus et al., 2007), isolated groundwater NOM (Artinger et al., 2002), and natural soil humic colloids (Crancon et al., 2010)). The degree of enhancement varied as did the solution and column experimental conditions. Each of these studies observed co-elution of U and NOM which (supported by modeling or ultrafiltration) led to the inference that the U-NOM complex was the mobile species. Co-elution alone does not

directly provide the U-NOM concentration, nor does it shed light on the mechanisms of U mobility enhancement. Modeling can be prone to inaccuracies in thermodynamic data or sensitivities to certain assumed or estimated parameters. Ultrafiltration can be problematic for separating the U-humic complex at near neutral pH range of this study. A number of researchers (Semiao et al., 2010, Czerwinski et al., 1994, Newman, 2011) have observed significant sorption of U to the membrane filters. Improved ability to quantify nanoparticle- and NOM-associated metals would improve assessments of the impact of metal speciation on transport at the bench and field scales.

This paper describes a series of static column tests of U transport through silica sand and hematite coated silica sand where the U-NOM complex was directly examined by symmetrical flow field-flow-fractionation (FFF) with online inductively coupled plasma-mass spectrometry (ICP-MS) elemental detection. **During FFF fractionation, colloids such as NOM,** along with any complexed metals, **are retained in the FFF channel and directed to the ICP-MS detector while uncomplexed metals exit the system via the cross-flow and thus are not analyzed.** FFF-ICP-MS adds a key ability to examine the role of the organic complex in U transport due to its unique ability to probe the absolute and relative amounts of U and DOC in each effluent sample. Examining the relationship between complexation and mobility involves four steps which we present in the Results sections: 1) conduct transport experiments and calculate breakthrough and recovery to understand bulk transport trends; 2) analyze effluent samples by FFF-ICP-MS; 3) measure specific UV absorbance (SUVA) on effluent samples in order to calibrate UV-DOC correlation in FFF-ICP-MS measurements; 4) compare FFF-ICP-MS measurements with bulk analyses.

2. Experimental Section

2.1. Experimental Design, Nomenclature, and Motivation

A series of 1D static column experiments were designed to test the effect of pH, surface mineralogy, and system history on U mobility and remobilization by SRHA, and to test the applicability of FFF-ICP-MS to quantify and characterize effluent U-HA complexes. The characteristics that varied among the experiments were system pH, SRHA concentration, U concentration, type of sand (silica sand, SS, or hematite coated silica sand, HCS), and system history. The influent solution

pH (4 or 5) was selected as an environmentally relevant pH range where the U-SRHA complex has been previously demonstrated to be a major species (Crancon et al., 2010).

Static columns were selected as the testing apparatus over the more common and traditional advective column. Static columns have found limited application in the study of metal transport (Tinnacher, 2008); more often, they have been used to examine transport of cells and viruses in porous media (Ryan et al., 2002, Scholl and Harvey, 1992, Scholl et al., 1990, Loveland et al., 1996). The approach was selected for the ease of construction and sampling, the ability to control both residence time and the number of pore volume exchanges, and the desired representative larger volume (but lower resolution) effluent sample. The resulting plots of U and DOC as a function of pore volume are termed pseudo-breakthrough curves (PBTC) because they are similar to traditional breakthrough curves in that they account for all eluted material, but points along the curve are at lower resolution due to mixing in the column and higher volume sampling.

Each column was subject to 2 or 3 pore volume (PV) loadings of experimental solution (containing U and/or SRHA). In between each experimental solution pore volume, multiple pore volumes of pH adjusted electrolyte were exchanged. Throughout this paper, we refer to the loadings of experimental solution as experiments, and identify each experiment by the column (A through F) and a numeral indicating whether it was the 1st, 2nd, or 3rd experiment carried out on that column. Table 1 summarizes the solution and column characteristics of each experiment. For example, the influent solution in Experiment C2 was pH 5 and contained 25 mg L^{-1}SRHA and 1 μmol L^{-1} U. Furthermore, it is at times useful or necessary to identify the individual point sample on the PBTC. As will be described in *Methods*, samples were usually collected in quarter PV increments. When discussing point samples or a region of the PBTC, the naming convention is to identify the column with the nominal pore volume as a subscript. For example $E_{6.25}$ refers to the PV 6.25 collected from column E and $C_{2.75\text{-}4}$ refers to the all the samples collected between PV 2.75 and 4. The region of the PBTC where each experiment's peak ought to elute assuming ideal transport through the column (not always the case) is also listed in Table 1.

2.2. Materials and material characterization

2.2.1. U complexation with NOM

All U solutions and standards were diluted from a stock solution of 1000 μg mL^{-1} uranyl nitrate (High Purity Standards, Charleston, South Carolina, USA). Dilutions for experimental solution were made in DI water while dilutions for ICP standards were made with 1% v/v HNO_3 (Optima trace metal grade).

Humic acid used for complexation and transport experiments was Reference Suwannee River Humic Acid (SRHA) obtained from the International Humic Substances Society (IHSS), catalog number 1R101H. The freeze-dried SRHA was typically dispersed in a stock solution of 250 to 700 mg L^{-1}, with a few drops of 0.1 M NaOH if necessary for dissolution. Stock solutions were used for a period of 2-3 months, and kept in amber glass containers and at 4^{o} C when not in use. The concentration of the SRHA solution was calculated from the masses of dry SRHA and DI water measured before dispersion, and confirmed by total organic carbon (TOC) analysis on a Shimadzu TOC 5000 Carbon Analyzer (Shimadzu, Columbia, MD, USA).

2.2.2. Sand preparation and characterization

The SS was obtained from U.S. Silica (type Q-ROK #1, Frederick, MD, USA) and treated to an extensive cleanup regimen by Tinnacher (2008), including sieving, combustion, and acid and base washing (see Electronic Annex for further details). QEMSCAN analysis (automated SEM with EDX) of 277 grains measured most particles between 200 and 500 μm and 99.8% of the surface area to be quartz. The most common impurities were unidentified clays (0.1%), potassium feldspar (0.02%), muscovite, titanium dioxide, and iron oxide (all $\leqq$ 0.01%).

A 170 g subsample of the SS (enough for constructing two columns plus extra for characterization) was coated with nanoparticulate hematite (nano-hematite). The coating technique was based on the procedure of Rusch et al. (2010) with the following modifications. The 170 g SS was mixed with 63.25 ml hematite suspension in a Teflon beaker (3.8 g L^{-1} nano-hematite suspended in 10^{-3} M $HClO_4$, synthesized in-house according to (Lesher et al., 2009, Matijevic and Scheiner,

Table 1: Summary of Static Column Experiments

Column, sand		Experiment **1**	**2**	**3**
A, SS	Influent [HA], mg/L	0	25	
	[U], µmol/L	1	0	
	pH	5	5	
	Effluent pH range	5.6-6.9	5.6-6.4	
	Ideal peak elution	PV 2.75-4	PV 8.75-10	
B, SS	Influent [HA], mg/L	0		
	[U], µmol/L	1		
	pH	4		
	Effluent pH range	5.3-5.9	4.6-5.2	
	Ideal peak elution	PV 2.75-4	PV 8.75-10	
C, SS	Influent [HA], mg/L	25	25	25
	[U], µmol/L	1	1	0
	pH	5	5	5
	Effluent pH range	5.5-6.1	5.5-6.1	5.3-5.4
	Ideal peak elution	PV 2.75-4	PV 9.75-11	PV 15.75-17
D, SS	Influent [HA], mg/L	25	25	25
	[U], µmol/L	1	1	0
	pH	4	4	4
	Effluent pH range	4.7-5.2	4.5-4.8	4.5-4.7
	Ideal peak elution	PV 2.75-4	PV 9.75-11	PV 15.75-17
E, HCS	Influent [HA], mg/L	25	200	
	[U], µmol/L	1	0	
	pH	5	5	
	Effluent pH range	5.0-5.3	5.3-5.6	
	Ideal peak elution	PV 3.75-5	PV 10.75-12	
F, HCS	Influent [HA], mg/L	50	200	
	[U], µmol/L	1	0	
	pH	5	5	
	Effluent pH range	5.2-5.4	5.2-5.3	
	Ideal peak elution	PV 3.75-5	PV 10.75-12	

The solution and matrix conditions for each column and experiment (A1, A2, B1, C1, etc.) are listed, along with the influent pH condition, the observed effluent pH range, and the PBTC region where the peak would be located assuming ideal transport.

1978, Penners and Koopal, 1986)), giving the equivalent of 1000 μg Fe per gram SS. The mixture was stirred vigorously by hand for approximately 5 minutes, then covered tightly and shaken for 2 h. After 2 h, the hematite coated silica sand (HCS) was rinsed in DI water until the rinse water was clear and then another 5 times. Air-dried HCS was digested in hydrochloric acid to find the coating density: 320 μg Fe dissolved off per gram HCS (compared with 20 μg Fe per gram of uncoated SS). A detachment study found that the hematite nanoparticles would not dissolve and/or detach from the sand under background electrolyte conditions. Specific surface area was measured by BET analysis (N_2 adsorption); coating the sand with hematite nanoparticles increased the surface area from 0.069 to 0.26 $m^2\,g^{-1}$. For the silica sand, an assumption was that the silica sites would dominate U sorption, since the QEMSCAN results indicated 0.2% of the surface was impurities. For the HCS, silica and iron oxide sites may play a role in binding U but it was hypothesized that iron oxide sites will dominate due to their high affinity for binding U. Details on these characterizations and resulting assumptions can be found in the Electronic Annex.

2.3. Methods

2.3.1. Static column construction

Flow through the static column is dictated by gravity and the opening and closing of valves. Essentially, it is a hybrid of a batch sorption experiment and an advective column. Like a batch sorption test, the residence or equilibration time between porous media and experimental solution can be strictly controlled. Like an advective column, the solid-solution ratio is reflective of aquifer conditions, and when pore volumes are exchanged, solution moves through the column as it would in an advective system, however flow rate is not controlled.

Six static columns were prepared to test U transport through SS and HCS under various solution conditions. The design of the static columns was based on Tinnacher (2008), but upscaled by a factor of 2.5 to contain 82.5 g sand. The static column consists of a reservoir and the column itself, both with one-way stopcocks on their outlets to control flow. Electrolyte tracer tests (one pore volume 0.01 M $NaClO_4$ introduced in between pore volumes of DI water while monitoring effluent conductivity) were conducted on each column to ensure reproducible flow conditions between

columns, and to have a baseline elution profile. The exact dimensions, components, and directions for construction, packing, and tracer testing can be found in the Electronic Annex.

2.3.2. Loading and elution of experimental solutions

Upon completion of the tracer test, the general procedure for conducting a transport experiment consists of equilibrating the sand matrix with electrolyte solution, loading the experimental solution, and elution - exchanging pore volumes with electrolyte solution. The general procedures were based on Tinnacher (2008). After the tracer test, 0.01 M $NaClO_4$, adjusted to either pH 4 or 5 and hereafter referred to simply as "electrolyte," was used for all PV exchanges in between experiments.

Before loading the experimental solution, one PV electrolyte was loaded and allowed to equilibrate for at least 60 min. Then a second PV of electrolyte was exchanged in half PV increments. Finally, the experimental solution was loaded (and background samples collected) in quarter PV increments. The last quarter PV collected typically contained components of the experimental solution because of the advective-dispersive broadening of the slug; this sample is termed the Load sample. After loading, the system was allowed to equilibrate for 72-73 h. Following equilibration 2 PV electrolyte were exchanged, with samples again collected at quarter PV increments. Two more PV were exchanged 18.5-19 h later. This relatively short delay tests for any rebound in analyte concentrations which if seen, might indicate desorption or a diffusion based mass transfer limitation.

The PBTC is delineated into the Peak and Tail regions based on when a non-reactive tracer would elute: the Peak is defined as the pore volume collected directly after one pore volume of experimental solution was loaded. The Tail is any effluent collected after Peak elution. The two regions of the PBTC are used for the relative recovery calculations presented in *Results*. The Load sample is considered part of the Peak region for recovery calculation, but it is important to note that the Load sample is fundamentally different from the later Peak samples that equilibrated with the sand; data shedding light on those differences will be discussed in *Results*.

2.3.3. Bulk analyses on effluent samples

The column effluents were characterized for pH, UV absorbance, TOC, total [U] and [Fe], and colloidal U content (this last analysis by FFF-ICP-MS). Details regarding instruments employed,

volumes required, and method notes can be found in the Electronic Annex. UV absorbance and TOC were used to calculate Specific UV Absorbance, SUVA ($L\ mg^{-1}\ cm^{-1}$), where

$$SUVA = \frac{UV\ abs_{254}\ \left(cm^{-1}\right)}{DOC\ \left(mg\ L^{-1}\right)} \quad (1)$$

Because SUVA is a normalized parameter, units are meaningless and thus not reported throughout.

2.3.4. Fl FFF-ICP-MS analyses on effluent samples

The effluent samples were analyzed for hematite nanoparticles, U bound to hematite nanoparticles, SRHA, and the U-SRHA complex using two separate FFF-ICP-MS methods. The FFF-ICP-MS method for nano-hematite fractionation, developed in Lesher et al. (2009) and hereafter referred to as the hematite FFF method, employs a relatively weak cross-flow field and concurrent ^{238}U and ^{57}Fe ICP-MS monitoring (all ICP-MS analyses were conducted on a PerkinElmer Elan 6100). The method for SRHA separation and U-SRHA quantification was developed for this work and detailed in Lesher (2011) and uses a stronger cross-flow field and concurrent ICP-MS ^{238}U measurement and UV detection for the NOM. It is referred to as the NOM FFF method. In summary, both methods rely on converting the fractogram from net intensities to concentrations by comparison to a calibration curve of 0.01, 0.1, 1 μg L^{-1} for U and 1, 10, 100 μg L^{-1} Fe. The measured flow rate, q, was used to integrate the curve to yield masses of fractionated Fe and U. For U masses, a preceding blank run (of equal SRHA concentration) was subtracted out due to the ability of SRHA to scavenge previously deposited U from the FFF membrane. The ICP-MS was tuned and optimized daily to achieve the highest monitoring element (Rh, Pb, In) counts, so some parameters (such as nebulizer flow rate, detector voltage, etc.) changed over the course of experimentation. Further details related to ICP-MS operation, metal quantification, and data processing can be found in the Electronic Annex.

In a test mixture of 100 mg L^{-1} SRHA and 100 mg L^{-1} hematite, the hematite FFF method resulted in UV and Fe fractograms characteristic of the mixed sample: a very large UV peak that also contained an Fe signal (likely void peak NOM and Fe, the Fe coming mostly from unfractionated hematite, but also possibly Fe ions stripped off the hematite by the NOM), followed by a second

UV and Fe peak representing the fractionated nano-hematite. The second peak was determined by FFF theory (Giddings et al., 1976, Giddings, 1993, Schimpf et al., 2000) to be composed of particles 52 nm in diameter on average, which is consistent with the previous measurements of the nano-hematite.

The hematite FFF method was only run on the three effluent samples with the highest bulk Fe concentration: $E_{11.75}$, $F_{11.75}$, and F_{12} (these samples are from Experiments E2 and F2) to test for the presence of nano-hematite and/or nano-hematite associated U. All samples from Experiments C1, C2, C3, D1, D2, D3 and selected samples from Experiments A2 and B2 were run using the NOM FFF method to analyze for SRHA and SRHA associated U. The effluent samples from Experiments E2 and F2 (and some from E1 and F2) were run using the NOM FFF method to test for SRHA, SRHA associated U, and SRHA associated Fe.

3. Results and Discussion

Bulk results, in the form of pseudo-breakthrough curves and relative mass recoveries calculated from the PBTCs, indicate significantly enhanced U transport when U is preequilibrated with SRHA. Among these experiments, greater recovery was observed with the pH 5 influent solutions compared to pH 4. Experimental and electrolyte solutions pH were not buffered, leading to some variability as summarized in Table 1 (the full dataset of pH as a function of pore volume can be found in the Electronic Annex). Transport through the column and the associated equilibration with the sand matrix resulted in increased pH of the effluent compared to the influent. For all columns, the relative mass recoveries are presented in tables; absolute mass loadings and recoveries (from which the relative recoveries were calculated) can be found in the Electronic Annex. These results are followed by the FFF-ICP-MS identification of the U-humic complex as the mobile species and SUVA characterizations of column effluent that demonstrate a fractionation of the organic matter, with the more highly absorbing fractions retained by the media.

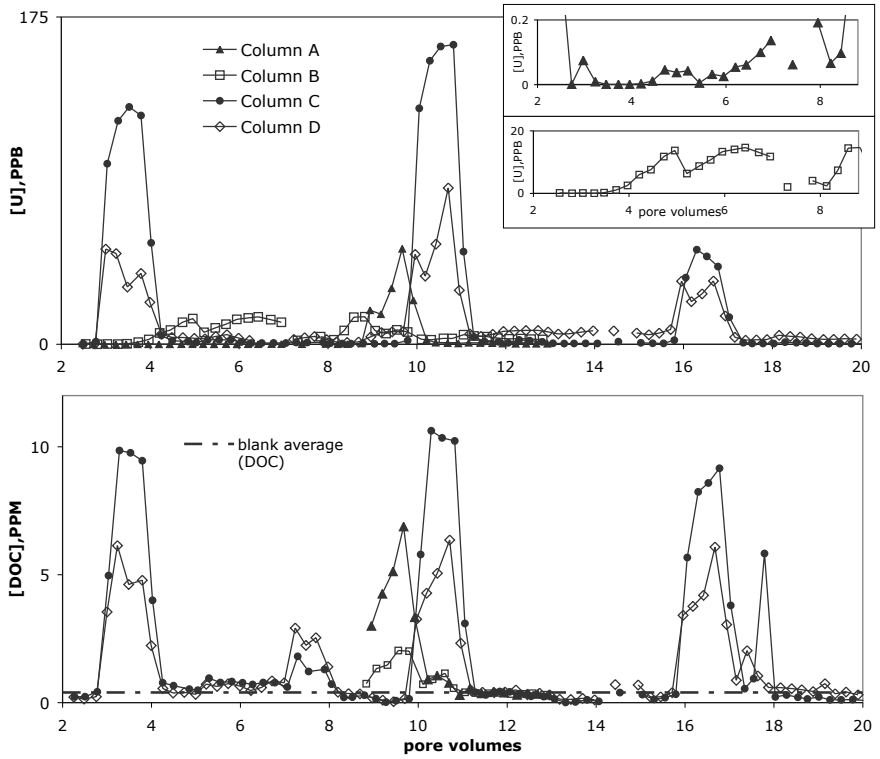

Figure 1: PBTC: U and DOC Transport Through SS, Col A-D, Full Results

Columns A-D Pseudo breakthrough curves (top: U, bottom: DOC). The inset figures magnify the U PBTC in Experiment A1 and B1. The lack of SRHA in the influent solutions resulted in retarded, low-level uranium breakthrough (ideal breakthrough would occur between PV 2.75 and 4). Not that DOC was not measured until A_9 and B_9 since the influent solution in Experiments A1 and B1 did not contain any SRHA.

3.1. Breakthrough and Recovery of Uranium and DOC Through Silica Sand Columns

Uranium Transport. The breakthrough of uranium through SS columns was significantly enhanced by pre-equilibration with SRHA and was dependent on system pH. Very little of the uranium in Experiments A1 and B1 (no SRHA) eluted, as is illustrated in Figure 1(top) and quantified in Table 2. In Experiment B1 (influent pH of 4), 25.4% of loaded U broke through, but the transport was retarded, with most of that eluting during the tail. Only 0.41% of the loaded U was recovered from Column A. The mechanism of retention in both columns was U adsorption to silica sites, likely through ligand exchange with a protonated surface site.

The difference observed between Experiments A1 and B1 is to be expected. At the lower pH, the

Table 2: Relative Recoveries of Uranium, All Columns

		Col A	**Col B**	**Col C**	**Col D**	**Col E**	**Col F**
Peak 1	mass U loaded, μg	3.73	5.18	7.62	8.05	7.16	7.91
	peak only %recovery	0.02%	0.57%	53.4%	18.4%	0.01%	8.69%
	peak+tail %recovery	0.41%	25.4%	56.2%	25.5%	0.06%	12.6%
	remaining U, μg	3.71	3.87	3.34	5.99	7.15	6.91
Peak 2	mass U loaded, μg	0	0	7.26	7.21	0	0
	peak only %recovery	*27.5%*	*8.22%*	***48.6%***	***15.2%***	*49.6%*	*48.9%*
	peak+tail %recovery	*29.2%*	*16.2%*	***50.2%***	***22.4%***	*50.2%*	*49.3%*
	remaining U, μg	2.63	3.24	5.27	10.25	3.57	3.50
Peak 3	mass U loaded, μg			0	0		
	peak only %recovery			*9.75%*	*6.66%*		
	peak+tail %recovery			*10.1%*	*8.56%*		
total	%recovery	29.5%	37.5%	74.6%	78.4%	50.2%	55.7%

Italics indicate remobilization. Remobilization is calculated as the mass of U eluted in the given peak (see Electronic Annex) ÷ "remaining U," the mass of U remaining in the column after the previous peak elution. Bold italics indicate the recovery is comprised of U introduced by the 2nd experiment, as well as U deposited by the first experiment and remobilized: Peak 2 subtotal ÷ [remaining U (from Peak 1) + Peak 2 "mass of U loaded"]

SS is more protonated, thus reducing the available silicol binding sites. The observed retardation in Experiment B1 presents an inverse relation between residence time and U desorption, which is more easily observed by enlarging the elution profiles (bottom inset of Figure 1). If the transport through the column was ideal, the peak would elute between $B_{2.75\text{-}4}$ (as as noted in Table 1). The effluent collected in $B_{2.75\text{-}4}$, that had been equilibrating for 72 h, was low in [U] ($<$2.55 μg L^{-1}), while $B_{4.25\text{-}5}$ (mostly fresh electrolyte solution that had *not* been in contact with the sand for 72 h) steadily climbed with each subsequent quarter PV collected. $B_{5.25\text{-}7}$ were collected 18.5 h later, and a similar increase in effluent [U] was observed as the equilibrated electrolyte was replaced by fresh electrolyte, until a shift downward was observed at $B_{6.75}$. The same trend was observed in Experiment A1, but the concentrations are two orders of magnitude smaller, peaking at 0.19 μg L^{-1} at A_8 (top inset of Figure 1).

The recovery of U in the presence of 25 mg L^{-1} SRHA is also pH dependent, but the trend is reversed from Experiments A1 and B1, where the lower pH increased U recovery. Figure 1 (top) and Table 2 illustrate the U recoveries in Columns C (influent at pH 5) and D (pH 4). Experiment C-1 saw the recovery of 56.2% of loaded U, compared to 25.5% in Experiment D1. Presumably, and as has been shown in previous modeling and experimentation (Lenhart et al., 2000), the higher pH

of solution C1 promotes formation of the U-SRHA complex to a greater extent than in D-1**,** where there is relatively more uncomplexed U and uncomplexed HA. However, in both solutions there is an order of magnitude more HA than U on a molar basis (see Electronic Annex for calculations), so the concentration of uncomplexed HA is relatively constant. The difference in recoveries between Experiments C1 and D1 suggests that the U-SRHA complex is responsible for enhanced transport, but support for that conclusion will be discussed in more depth following presentation of the FFF-ICP-MS identification of the U-SRHA complex.

C2 and D2, which were duplicates C1 and D1, presented an opportunity for the NOM to both enhance elution of U introduced with the NOM, and to remobilize the U deposited on the sand by the previous experiments. The mass of U recovered was greater in C2/D2 as compared to C1/D1 (masses listed in Electronic Annex). But the relative recovery (in bold italics on Table 2), which is the peak mass divided by all of potentially mobile U (the mass of U loaded in C2/D2 plus the mass of U remaining after C1/D1), indicates reduced mobility. A possible explanation is that the fraction of the U sorbed during Experiments C1 and D1 is held in stronger surface complexes and is less able to be remobilized.

The influent solution in A2 and B2 was 25 mg L^{-1} SRHA without any U. The resulting peaks saw the remobilization of 29.2% and 16.2%, respectively, of the previously deposited U. The third and final influent solutions introduced to Columns C and D were also 25 mg L^{-1} SRHA without any U; C3 and D3 remobilized 10.1%, and 8.56% of the previously deposited U, respectively.

DOC Transport. The DOC PBTCs indicate that the SRHA is being retained on the SS; recovery is significantly less than 100% in most cases. Figure 1 (bottom) shows the complete results of DOC measurements on Columns A-D effluent samples. Since Experiments A1 and B1 were free of SRHA, DOC was not measured until the loading and elution of Experiments A2 and B2 at PV 9.

TOC analysis on 17 effluent samples from the columns before the introduction of SRHA ("column blanks") gave an average DOC of 0.24 mg L^{-1} with a standard deviation of 0.16 mg L^{-1}. The value of the column blank average value plus one standard deviation ($\mu + \sigma = 0.40$ mg L^{-1}) is plotted as a dashed black line on Figure 1 (bottom). It is not recommended to quantify directly with

Table 3: Relative Recoveries of DOC, All Columns

		Col A	**Col B**	**Col C**	**Col D**	**Col E**	**Col F**
Peak 1	mass DOC loaded, mg			0.32	0.32	0.31	0.62
	peak only %recovery			90.0%	49.8%	14.7%	24.6%
	peak+tail %recovery			114.6%	79.4%	28.4%	33.7%
Peak 2	mass DOC loaded, mg	0.27	0.30	0.31	0.31	1.97	1.97
	peak only %recovery	58.2%	16.3%	98.6%	50.9%	113.2%	115.9%
	peak+tail %recovery	65.5%	23.1%	100.0%	57.4%	113.8%	117.0%
Peak 3	mass DOC loaded, mg			0.27	0.30		
	peak only %recovery			97.1%	49.8%		
	peak+tail %recovery			115.5%	63.6%		
total	%recovery	65.5%	23.1%	109.8%	66.9%	102.0%	97.1%

Relative recoveries are with respect to the DOC loaded with the peak/elution in question. Any uneluted DOC remaining from previous elutions was not considered during the calculation of %recovery of a given peak, since it was hypothesized that any SRHA lost to the sand would not be "remobilized" by subsequent SRHA injections, however recoveries in Experiments E2 and F2 were significantly greater than 100%.

measurements below this value. Furthermore, the DOC of the stock experimental solutions for Columns A and B, prior to column transport, were 0.29 and 0.17 mg L^{-1} DOC respectively; these values are quite close to the average column blank and likely indicate that DOC is contributed by the vials or stock solution preparation methods, and that it is difficult to distinguish between DOC contributed by the columns *versus* the vials and other solution handling steps.

Because of consistent DOC bleed of a few tenths of a mg L^{-1}, the measured DOC concentrations shown in Figure 1 (bottom) were adjusted prior to calculation of DOC recoveries. Values that were less than 0.40 mg L^{-1} were treated as below detection limit, and the DOC mass contributions not counted towards the peak and overall recoveries. For values greater than 0.40 mg L^{-1}, the blank average 0.26 mg L^{-1} was subtracted from the measurement prior to calculating the mass of DOC recovered in that particular quarter or half PV sample. These adjusted results are reported in Table 3. This adjustment makes the DOC values more reflective of elution of SRHA and not low level DOC that may leach from the sample vials, sand, column components, or non-SRHA DOC in the influent stock solutions.

The relative DOC masses (Table 3) show that loadings of Experiments A2 and B2 resulted in DOC recoveries of 65.5% and 23.1% respectively. C1, C2, and C3, each containing 25 mg L^{-1} SRHA, resulted in approximately 100% recovery of the TOC in the main peak: 90.0%, 98.6%, and

97.1%. Overall recovery was 109.8% considering the tails of the three peaks. In Column D, peak recoveries were less: 49.8%, 50.9%, and 49.8% (for D1, D2, and D3, respectively) with an overall recovery (including tails) of 66.9%. The lower recoveries of DOC in Columns B and D as compared to A and C are consistent with lower system pH.

There is a stark contrast between Columns A-B and Columns C-D with regard to NOM adsorption/transport. The variables differing between the influent solutions A2 and B2 and any of the Column C-D experiments were the presence of uranium in the influent, system history, and to a small degree, pH. The pH differences among the columns do not explain the divergent recoveries, as the B2 effluent pH falls in between that of the C and D column effluents, but it had the lowest recovery. The literature suggests lower pH enhances sorption of NOM to mineral surfaces, yet the pH of the Experiment A2 A effluent was the highest of the four, and recovery was much lower than in C1-3 and was approximately equal to that of the Column D experiments. Furthermore, tests of sorption of Suwannee River fulvic acid to this specific silica sand, carried out by Tinnacher (2008), showed little difference in sorption capacity for fulvic acid at the pH range studied here.

Discussion and Mutual Influence of U and DOC . If pH is not a controlling variable on divergent DOC recoveries between Columns A-B and C-D, system history, including the presence of U cations in the C1 and D1 influents, may play a role. It is possible that cation bridging, where sorption of U onto the sand during Experiments A1 and B1 could increase the subsequent sorption of NOM, is occurring, but the molar amounts of sorbed U would not significantly impact the mass of DOC transported. We hypothesize that the dissolved U(VI) in C1, C2, D1, and D2 stabilize the SRHA and makes partitioning to the silica surface less favorable. In other words, that the U-SRHA complex is more mobile in the columns than the SRHA by itself. This hypothesis requires more testing and more control on pH and time in between subsequent experiments on a given column.

The results presented above clearly demonstrate that SRHA enhances the mobility of U. However, there are two possible explanations: either (1) the new SRHA is removing the previously sorbed U from the column (while the new U is partitioning to the sand at the same proportions it did in the first experimental pore volume), or (2) less of the newly introduced U is partitioning to

the sand. Because our calculations show that there is an excess of total silica sites compared to the previously introduced SRHA and U, and little of the SRHA was retained, it is unlikely that fewer available silica sites would reduce the partitioning of the newly introduced U (explanation 2), so explanation 1 is more likely. Looking specifically at Columns C and D, Column C has a greater recovery of both U and DOC. The lower pH of Column D does not promote the U-SRHA solution complex to the degree that the higher pH Column C does, and the silica surface is more reactive towards NOM. But, the amount that did stay in solution likely picked up some of the U previously deposited on the sand. When only NOM was introduced to Columns C-D (Experiments C3 and D3), more U was remobilized from Column C in both relative and absolute terms. This is likely a result of the increased importance of the U-SRHA solution complex at the increased pH, and the lack of affinity of the silica surface for SRHA at the higher pH.

3.2. Breakthrough and Recovery of U, Fe, and DOC Through Hematite Coated Silica Sand Columns

The breakthrough of both U and SRHA through the HCS columns was very limited in experiments E1 and F1.However, the second loadings onto these columns (E2 and F2) contained 200 mg L^{-1} SRHA, and mobilized significant amounts of U. **This concentration of organic matter was selected with U mobilization as a goal, but also represents the upper end of DOC concentrations found in natural systems or a DOC typical of wastewater. Furthermore, lower DOC systems can exhibit temporal and spatial variability in DOC concentrations, perhaps resulting in spikes to similar concentrations** (Jaffé et al., 2008, Worrall et al., 2004). The mechanisms at play in Columns E-F are essentially the same as with the previous columns, except that the increased surface area and increased affinity of the hematite particles for both NOM and uranium relative to the silica increases surface sorption and decreases U and SRHA transport. The PBTCs for U, Fe, and NOM are shown in Figure 2. Only small masses of Fe, for which ICP-MS detection is noisy and insensitive (detection limit of 1-10 $\mu g\, L^{-1}$), were mobilized by the NOM. The nature and amount of the mobilized Fe is discussed in Subsection 3.5.

The relative recovery of U for Columns E and F is presented in Table 2. Unlike the Column C experiments, where at a similar pH (see Table 1) 25 mg L^{-1} SRHA showed a capacity to transport

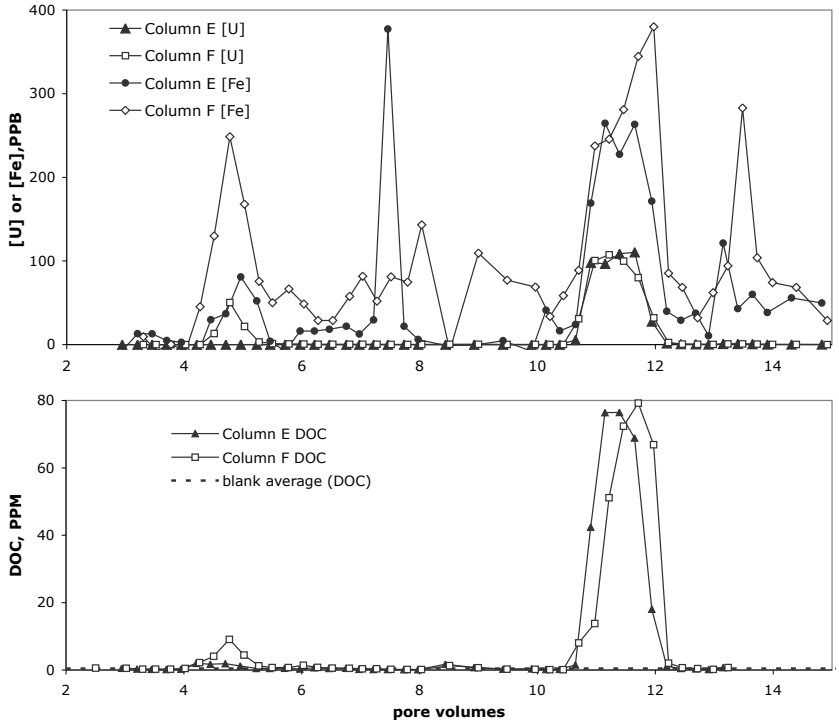

Figure 2: PBTC: U, Fe, (top) and DOC (bottom) Transport Through HCS, Col E-F, Full Results Columns E-F Pseudo breakthrough curves (top: U and Fe, bottom: DOC).

upwards of 50% of introduced U, in Experiment E1, less than 0.1% of introduced U broke through. In Experiment F1, 50 mg L^{-1} SRHA allowed for recovery of 12.6% of the introduced U. The slug of 200 mg L^{-1} SRHA in E2 and F2 mobilized about 50% of retained uranium in both Columns E and F. The masses mobilized (3.55 μg and 3.38 μg for E and F respectively, see Electronic Annex table) reflected that there was more U present to be mobilized in Column E since less eluted in the first peak.

The same adjustments for the DOC recovery calculations for Columns A-D were applied to the Column E and F mass integrations and recovery calculations tabulated in Table 3. In E1 and F1, the HA, like the U, was retained. The PBTC shows little DOC breakthrough : 28.4% and 33.7% for E1 and F1. Given that there was little HA retention in the pH 5 SS system (Experiments C1 and C2), it is likely that the SRHA is predominantly sorbing to FeO sites. **The lack of interpeak tailing in Column E is a sign of the strength of both U and HA sorption to the FeO sites.**

The intent of the 200 mg L^{-1} SRHA influents in E2 and F2 was to mobilize larger masses of U and Fe that, ideally, would produce samples that could be characterized for U and Fe by FFF-ICP-MS. The DOC recoveries from E2 and F2 were 113.8% and 117%, which made the overall DOC recovery (accounting for both experiments in both columns) 102% and 97.1%. **These values indicate that E2 and F2 remobilized the previously deposited DOC.**

3.3. UV Characterizations of Effluent Samples (Columns A-F) - Effect of System History/Conditioning

SUVA measurements on column effluent and samples collected before introduction to the columns suggest that NOM undergoes compositional changes during transport. In the experiments with high recovery of DOC (greater than 60%), SUVA measurements on the effluent samples were constant over the elution of the peak, while in the peaks with lower recovery, the SUVA elution profile (Figure 3) varied between the samples that comprise the peak. Furthermore, peaks with greater recoveries of DOC have higher SUVA, as is shown in Figure 4. In this comparison, the SUVA values of the four quarter PV effluent samples that eluted after the 72 h equilibration were averaged (outlined by black boxes in Figure 3 and hereafter referred to as "peak SUVA"). The average

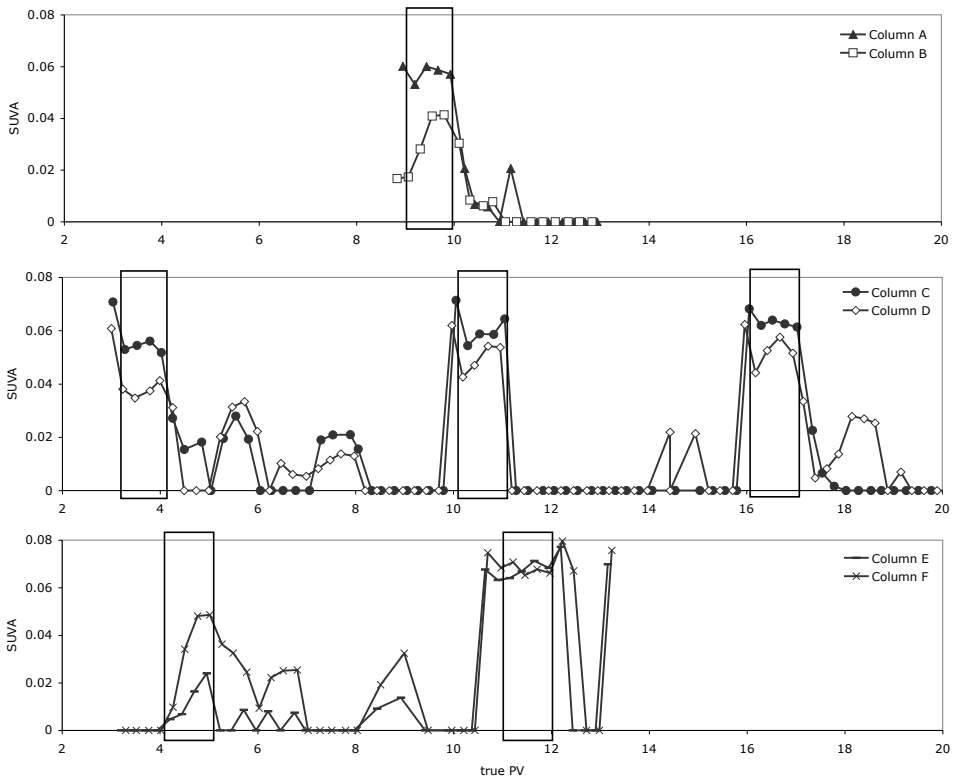

Figure 3: SUVA Characterization of DOC Breakthrough, where DOC > 0.5 mg l^{-1}

The peak SUVA is outlined in black boxes (does not include the preceding Load sample, which is often slightly higher than the peak). The peak SUVA average is used in comparisons in Figure 4. The breakthrough plot also shows SUVA peaks on the smaller DOC peaks that eluted later. SUVA measurements where DOC ≤ 0.5 mg l^{-1} are plotted as 0 as they are not reliable due to detection limits on both the UV spectrometer and the TOC analyzer.

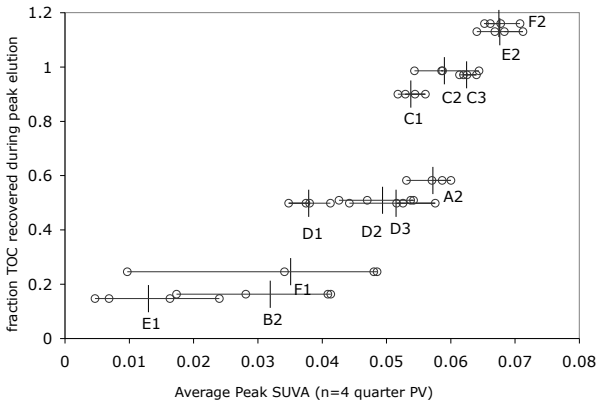

Figure 4: TOC Recovery as a Function of Peak $SUVA_{254}$, Columns A-F

Each peak has all four SUVA values (the four quarter PV measurements constituting one peak) plotted as points connected by a line. The vertical mark indicates the average of the four measurements. The height of the vertical mark represents $\pm$ 0.05 error to estimate the known lack of sensitivity of the TOC analyzer, upon whose measurements the the fractional recoveries were calculated. The range of values is greater for the low SUVA, low recovery samples as breakthrough was non-ideal. These results indicate fractionation with the more highly absorbing fractions being lost to the porous media surface.

peak SUVA is represented by the vertical line, while the four points that went into the average are displayed as points connected by a line to visualize the full range. The ordinate value on the plot, relative recovery, is the "Peak only %recovery" value from Table 3. The relative recovery includes the TOC contributed by the Load sample which did not equilibrate. The SUVA of this quarter PV was typically higher or equal to the SUVA of the equilibrated PVs, and was not included in the average as it was fundamentally different in nature due to the lack of equilibration.

Higher SUVA has been shown to indicate a greater degree of aromaticity, higher binding capacity, and higher molecular weight (Leenheer and Croue, 2003, Weishaar et al., 2003). That the SUVA is lower when less DOC makes it through the column suggests a fractionation of the humic acid, with the highest absorbing fractions of the SRHA preferentially sorbing to the sand, leaving the remaining solution phase DOC depleted in these fractions and exhibiting a lower SUVA.

In Figure 5, the SUVA of each peak is compared to each other peak and to the SUVA measurements of the Load sample, which passed through the column during loading and did not equilibrate for 72 hours, and to the SUVA of the influent solution before it had contacted the sand (not available for all peaks). Comparing the peak SUVA for subsequent loadings (possible only in Columns C-F)

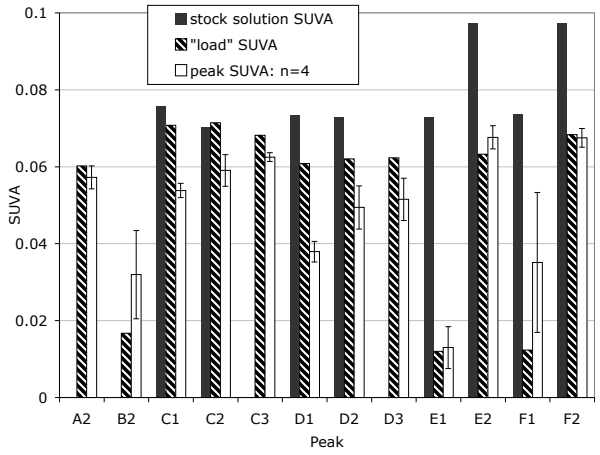

Figure 5: SUVA of "Peak," "Load," and Stock Solution Samples

"Peak" SUVA is the average SUVA of the four quarter PV samples that eluted after 72-73 hours equilibration (error bars are ± 1 standard deviation on the average calculation to show the range of the four samples). "Load" SUVA is the SUVA of the quarter pore volume of experimental solution that passed through the column during loading and did not equilibrate for 72 h. Stock solution SUVA measurements (where available) were taken on the experimental solution before contact with the sand.

indicates increasing SUVA with each sequential loading. The trend is especially strong in Columns E and F. An explanation for this observation is that as more NOM is introduced to the column, the sand surface gets more and more coated, and less able to bind the NOM. As more NOM makes it through the column, there is less partitioning to the sand surface occurring, so the effluent can be characterized as more aromatic.

In the peaks where recovery was greater than 60% (A2, all C and D experiments, E2, and F2), the Load SUVA was usually within or above the error bars on the peak SUVA. This suggests that fractionation of the NOM to the sand is not instantaneous; rather, prolonged contact with sand results in more fractionation. However, when the stock experimental solution was characterized for UV absorbance, the SUVA was usually greater than that of the Load; in a few cases (influent solutions E1 and F1), dramatically higher. In these columns, the short amount of time (typically 3-5 minutes) that the solution contacted the sand was enough to initiate the DOC fractionation process. This can be attributed to the presence of the hematite.

3.4. Identification of the U-SRHA Complex by FFF-ICP-MS

The NOM FFF method was applied to most Load and Peak effluent samples with DOC greater than 2 mg L^{-1}. The advantage of FFF-ICP-MS characterization of the column effluent is the ability to examine the U-HA complex directly, as any uncomplexed U exits the FFF channel via the cross-flow and was not analyzed by ICP-MS. The analysis resulted in U concentration fractograms (displayed in the Electronic Annex) and a UV absorbance fractogram. The U fractograms were integrated to determine the mass of U associated with the fractionated SRHA ($m_U\prime$, μg). From the UV fractograms and the bulk SUVA measurement, the relative DOC, $DOC\prime$ (unitless) is defined as

$$DOC\prime = \frac{UV\ area}{SUVA}$$

As described in the previous subsection, the lower pH columns and HCS columns caused SRHA fractionation during transport through the column resulting in lower SUVA of effluent samples. Therefore using UV area on its own as a proxy for DOC would result in underprediction of relative DOC.

The total set of $m_U\prime$, $DOC\prime$, and the ratio of those two measurements, $\frac{m_U\prime}{DOC\prime}$ for all measured effluent samples are depicted in Figure 6, where each panel corresponds to the experiment indicated in the top left of the panel. The x-axis labels on E2 and F2 apply to each plot, although influent values are not always available. The primary (left) y-axis label quantifies $m_U\prime$ (μg) and $DOC\prime$, and the secondary (right) y-axis label scales $\frac{m_U\prime}{DOC\prime}$. The significance of the $\frac{m_U\prime}{DOC\prime}$ ratio is that it is a proxy for measuring the U-SRHA complex and estimates how much U there is per mole of SRHA. As will be shown in the ensuing discussion, the value lends an insight into retardation and fractionation of SRHA and the corresponding influence on associated U transport, the effect of equilibration time on the transfer of U between SRHA- and sand-associated, and the remobilization of previously deposited U by SRHA.

The first observations can be made on samples from within a column set. In Column A, where a pore volume of only HA (A2) appears to have remobilized some of the previously sorbed U, $\frac{m_U\prime}{DOC\prime}$

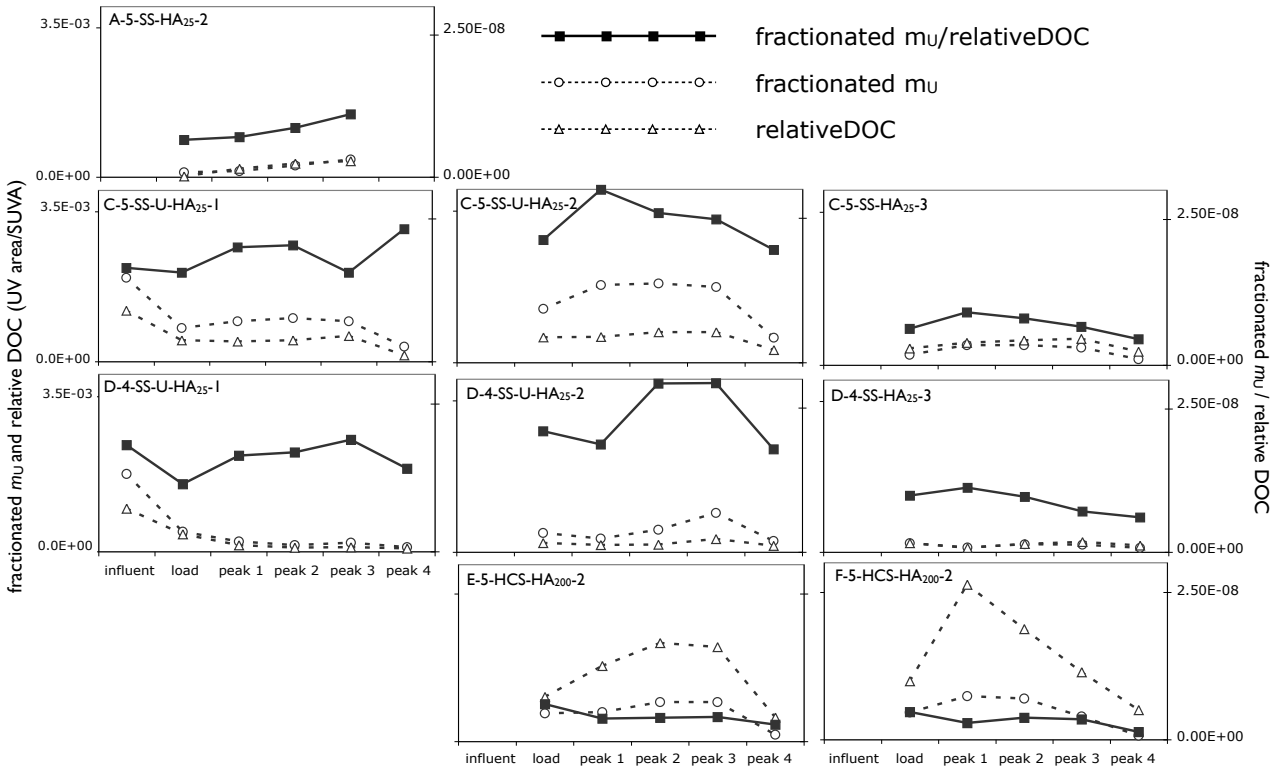

Figure 6: $DOC\prime$, $m_U\prime$, and $\frac{m_U\prime}{DOC\prime}$ values for all experiments (that yielded measureable amounts of U-SRHA complex) as a function of **peak positioning**. $DOC\prime$ and $m_U\prime$ values are plotted on the primary (left) y-axis for each panel, while $\frac{m_U\prime}{DOC\prime}$ is plotted on the secondary (right) y-axis. Influent values are not available for each Experiment.

increases over the elution profile. The Load sample (A_9) has the lowest ratio; it is marginally smaller than $A_{9.25}$, the first quarter PV eluted. This suggests two processes: (1) an increasing adsorption of HA to the sand over the course of elution, or (2) increasing desorption of U from the sand and subsequent complexation with the HA; or a combination of those two processes. Since $DOC\prime$ increases with each quarter PV (along with $m_U\prime$), option 1 can be ruled out. Since $\frac{m_U\prime}{DOC\prime}$ increases with each subsequent quarter PV, we hypothesize that increasing contact with the sand enhances U remobilization.

Within the set of Column C and D experiments, $\frac{m_U\prime}{DOC\prime}$ is higher for the second Experiments compared to the first (C2 *versus* C1, D2 *versus* D1). This is strong evidence for remobilization, as

the NOM is not only transporting the U complexed with it, but remobilizing some of the previously deposited U. Given the site calculations (Electronic Annex), we know that there are significantly more humate molecules compared to sorbed U ions, therefore this is a logical explanation.

In Columns E and F, the values of $\frac{m_{U}\prime}{DOC\prime}$ are much lower than in other columns because the influent solution contained more SRHA (200 mg L^{-1}) and no U; any U eluted was U that was remobilized. Interestingly, the Load values are higher than the post-equilibration effluents. In other words, a large amount of U was immediately desorbed from the HCS surface and complexed with the SRHA, but the time allotted for equilibration promoted re-dissociation and adsorption with the HCS. This suggests a fundamental, possibly kinetic, difference between the silica-U surface complex and the iron oxide-U surface complex.

Observations on the variations among and between column pairs where only one variable differed also gives insights into U transport mechanisms. Between Experiments C1 and D1, there is a lower $\frac{m_{U}\prime}{DOC\prime}$ ratio among most of the lower pH D samples, as would be hypothesized by models suggesting less formation of the U-SRHA complex at the lower pH. This observation supports the hypothesis that the U-SRHA complex is responsible for the transport of U through the column. However, the C2 and D2 $\frac{m_{U}\prime}{DOC\prime}$ values are not skewed higher in one column over the other. Most of these samples are higher than the C2 and D2 Load samples, suggesting a need for equilibration to remobilize the sorbed U. Finally, D3 samples are consistently higher than the C3 samples. This transition over the three experiments highlights the greater amount of sorbed U available for remobilization in Column D matrix compared to Column C. In Columns E and F, a similar trend exists, increasing $\frac{m_{U}\prime}{DOC\prime}$ in the E2 effluent samples as compared to the F2 samples because there is more U available to remobilize.

If FFF-ICP-MS characterizations are inherently more useful than the ratio the mass of U to mass of DOC in the bulk effluent samples ($\frac{m_{U}}{DOC}_{bulk}$) because the U-SRHA complex is measured directly and simultaneously), then it could follow that $\frac{m_{U}}{DOC}_{bulk}$ would differ from the FFF-ICP-MS measured $\frac{m_{U}\prime}{DOC\prime}$ ratio over the course of elution events. These differences are plotted for Columns C and D, Experiments 1-3 in Figure 7. To facilitate comparison, the $\frac{m_{U}\prime}{DOC\prime}$ and $\frac{m_{U}}{DOC}_{bulk}$ bars are scaled commensurately for the influent C1 and D1 solutions (which were measured never having

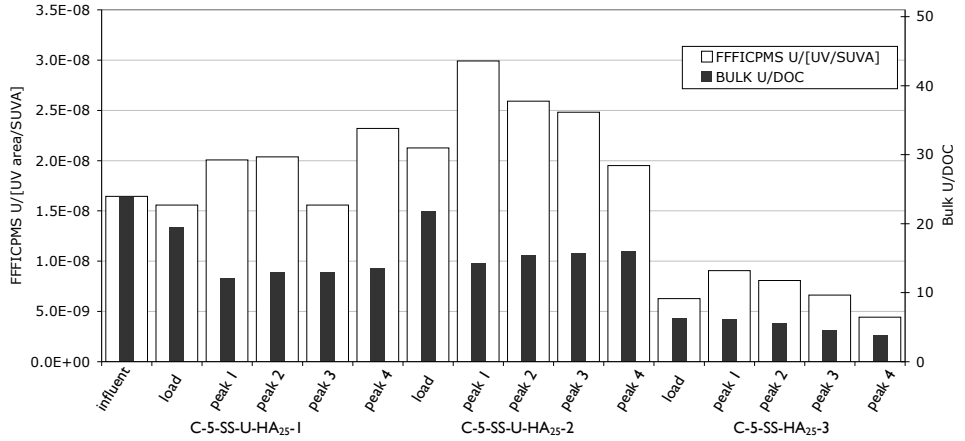

(a) C samples

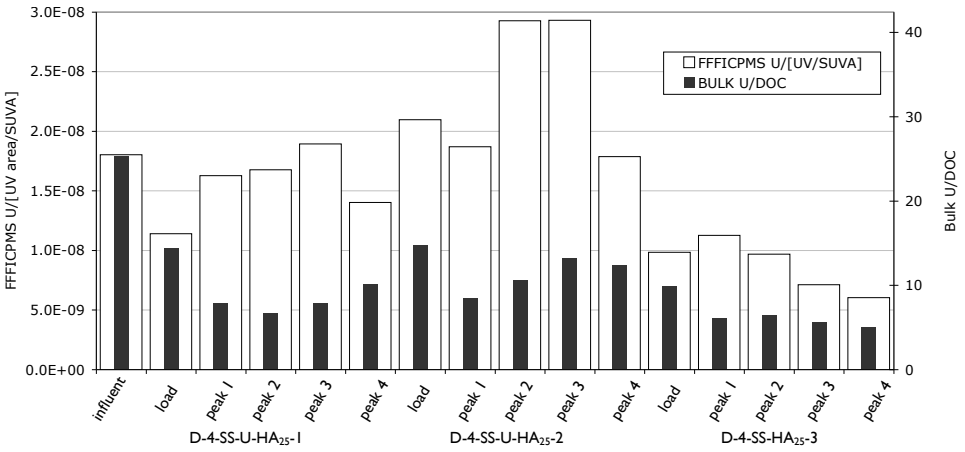

(b) D samples

Figure 7: FFF *Versus* Bulk Measures of the U-DOC Ratio

contacted the sand). While this scaling is arbitrary, the influent solution serves as a reference point for the effluent measurements that follow.

Focusing on the bulk data, the influent solutions result in the highest signal, followed by the Load samples for C1, D1, C2, and D2. This trend is not observed in the FFF ratios which are characteristic of only the complexed U. This divergence in trends indicates the presence of dissolved U in the influent solutions and Load samples.

The FFF ratios show somewhat more variability than the bulk ratios, and in some cases exaggeration of trends seen in the bulk data. For example, in Experiments C3 and D3, which represent the U remobilized by the SRHA, $\frac{m_{U'}}{DOC'}$ shows a clear downward trend over the four quarter PV peak samples. This is likely a result of increasing difficulty in remobilization. In other words, the introduced SRHA initially stripped off the weakly held U. As subsequent quarter PVs move through the column, there is slightly less U to be desorbed, and it is in stronger surface complexes. Another generalization that can be made is that the last quarter PVs (Peak 4 samples) collected tend to have a lower $\frac{m_{U'}}{DOC'}$ ratio than the previous quarter PVs. This could be due to tailing of less reactive, lower molecular weight fraction of the SRHA that is less able to scavenge sorbed U in this quarter PV.

Both of these observations support FFF-ICP-MS as a better method for tracking and characterizing movement of the U-HA complex.

3.5. Transport of Fe in HCS Columns

Overall, very little transport of Fe was observed in the HCS columns. The hematite nanoparticles remained adhered to the sand surface, despite the influx of, and equilibration with NOM. A question of interest was, "if Fe is released from the column, what form is it in?" The question was answered using the toolbox of FFF-ICP-MS methods described previously.

The hematite FFF method was only run on the effluent samples with the highest bulk Fe concentration: F_{12}, $F_{11.75}$, and $E_{11.75}$. None of these displayed an Fe peak near the time expected based on fractionation of a test mixture (100mgL^{-1} nano-hematite, 100mgL^{-1} SRHA, see Electronic Annex for more details), so it was concluded that if nano-hematite was removed from the sand

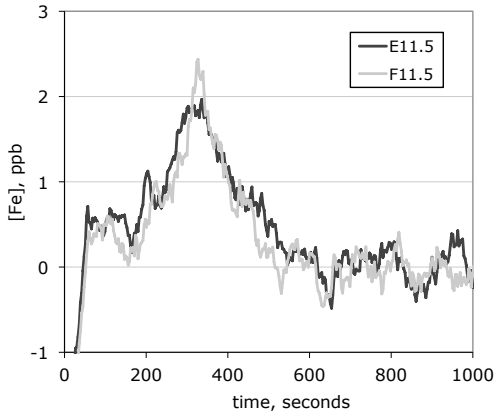

Figure 8: FFF-ICP-MS Fe Fractograms on Peak Samples from Columns E-F, Obtained Using NOM FFF Method

surface by the SRHA, it was then dissolved, degraded into a different form, or was only present at concentrations below the detection limit of the hematite FFF method.

All of the E and F effluent samples were run using the NOM FFF method. A small Fe peak was observed co-eluting with the NOM and U in most cases. Figure 8 shows the Fe fractograms for effluent samples $E_{11.5}$ and $F_{11.5}$ as examples of those that produced a discernible Fe peak. The noisy Fe baseline and weak sensitivity make the Fe measurements less useful than the U quantifications, but a small peak above baseline is present in these samples **which allows for qualitative interpretations of the results**.

We can conclude that the Fe is not in the form of detached nano-hematite. Rather, the signal results from Fe ions that have been solubilized from the HCS by the 200 mg L^{-1} SRHA influent solution, and are complexed with the SRHA. If the ions were not complexed with the HA, most of them would pass through the FFF membrane and not be measured, although it is not possible to rule out the presence of very small (<5 nm) iron oxide particles. NOM stabilized Fe has been previously observed in environmental samples (Krachler et al., 2010, Hassellov et al., 1999).

4. Summary

Effluent samples from tests of pH dependent transport of U, SRHA, and the U-SRHA complex through SS and HCS packed columns were characterized by traditional (total U, DOC, pH) and more advanced (effluent SUVA, FFF-ICP-MS) techniques. **Key results from this work include 1) observation of significantly enhanced U transport when U is preequilibrated with Suwannee River humic acid (SRHA) and at pH conditions promoting formation of the U-SRHA complex; 2) confirmation of the U-humic complex as the mobile species by FFF-ICP-MS and a dataset that shows compositional changes to the complex under varying transport settings; 3) a byproduct of the required UV-DOC calibration, SUVA characterization of column effluent demonstrates a fractionation of humic acid, with the more highly absorbing fractions retained by the media, and 4) identification of an iron-humic complex solubilized from the hematite coated sand. The results underscore the importance of organic complexation in studies of contaminant metal fate and transport, and present a novel tool for characterizing metal speciation in transport experiments.**

In the absence of NOM, U transport is retarded and recovery is very low, but is greater at lower pH. When SRHA is introduced to columns with sorbed U, a significant amount of U is remobilized. Recovery due to remobilization by SRHA is greater at the higher pH. Conditions promoting formation of the U-HA complex in the pre-equilibrated experimental solution (before injection, pH 5 *versus* 4) tend to enhance mobility and recovery of U. System history has a significant impact on the sorption of NOM to the sand surface, and hence its effectiveness in remobilizing previously deposited U. Coating silica sand with hematite nanoparticles drastically increases the sorption affinity of both U and NOM, however, slugs of concentrated NOM can still remobilize U in HCS columns. At the concentrations and masses studied here, the amount of U that can be scavenged and remobilized depends on the mass of previously deposited U.

The application of the advanced characterization techniques allowed for insights that could not otherwise had been extracted. Effluent SUVA characterization indicated fractionation of the NOM during transport, with high SUVA fractions preferentially adsorbing to the sand matrix. FFF-ICP-MS identified the U-HA complex as the mobile species in U transport when introduced to the

column as a mixture, and during remobilization events. This is an improvement over observation of contemporaneous U and DOC signals. Fluctuating U-relative DOC ratios in the fractionated subsequent peak samples suggests multiple types of U surface complexes of varying degrees of lability. Comparing the FFF-ICP-MS U-relative DOC ratios to the bulk ratio suggests uncomplexed U in the Load samples of Columns C and D, showing that without an equilibration period, dissolved U can pass through a column in the presence of NOM.

FFF-ICP-MS results give evidence for Fe-HA complex in HCS column effluent, suggesting that the experimental time frame results in NOM facilitated dissolution of iron oxide and complexation of Fe ions. Detached, intact nano-hematite from HCS was not observed in the column effluent (even when in contact with 200 $\mathrm{mg\,l^{-1}}$ SRHA), excluding nano-hematite as a significant vector for U transport in the studied systems.

FFF-ICP-MS has limitations that were exposed during this study, including poor recovery in the FFF channel, and the time-consuming nature of the procedure. But the ability to characterize the metal-NOM complex and measure the metal-NOM ratio are features that are useful in transport experiments where understanding the mechanisms of contaminant behavior is a goal.

Artinger, R., Rabung, T., Kim, J., Sachs, S., Schmeide, K., Heise, K., Bernhard, G., Nitsche, H., 2002. Humic colloid-borne migration of uranium in sand columns. Journal of Contaminant Hydrology 58 (1-2), 1–12.

Crancon, P., Pili, E., Charlet, L., 2010. Uranium facilitated transport by water-dispersible colloids in field and soil columns. Science of The Total Environment 408 (9), 2118 – 2128.
URL http://www.sciencedirect.com/science/article/B6V78-4YFT55P-2/2/ce2936c3c127ebde636a9d8d2f19777d

Czerwinski, K., Buckau, G., Scherbaum, F., Kim, J., 1994. Complexation of the uranyl ion with aquatic humic acid. Radiochimica Acta 65 (2), 111–120.

Davis, J., Coston, J., Kent, D., Fuller, C., 1998. Application of the surface complexation concept to complex mineral assemblages. Environmental Science & Technology 32 (19), 2820–2828.

EIA, 2011. Annual energy outlook 2011. Tech. rep., Energy Information Administration.
URL www.eia.gov/forecasts/aeo/

Giddings, J., Yang, F., Myers, M., 1976. Flow-field-flow fractionation: a versatile new separation method. Science 193 (4259), 1244.

Giddings, J. C., 1993. Field-flow fractionation: analysis of macromolecular, colloidal, and particulate materials. Science 260 (5113), 1456–1465.
URL http://www.sciencemag.org/cgi/content/abstract/260/5113/1456

Hassellov, M., Lyven, B., Haraldsson, C., Sirinawin, W., 1999. Determination of continuous size and trace element distribution of colloidal material in natural water by On-Line coupling of flow Field-Flow fractionation with ICPMS. Analytical Chemistry 71 (16), 3497–3502.

Jaffé, R., McKnight, D., Maie, N., Cory, R., McDowell, W., Campbell, J., 2008. Spatial and temporal variations in dom composition in ecosystems: The importance of long-term monitoring of optical properties. J. Geophys. Res 113, G04032.

Kazimi, M., Moniz, E., Forsberg, C., 2010. The future of the nuclear fuel cycle. Tech. rep., Massachusetts Institute of Technology.
URL web.mit.edu/mitei/docs/spotlights/nuclear-fuel-cycle.pdf

Krachler, R., Krachler, R., von der Kammer, F., Saphandag, A., Jirsa, F., Ayromlou, S., Hofmann, T., Keppler, B., 2010. Relevance of peat-draining rivers for the riverine input of dissolved iron into the ocean. Science of The Total Environment 408 (11), 2402–2408.

Leenheer, J., Croue, J., 2003. Peer reviewed: Characterizing aquatic dissolved organic matter. Environmental Science & Technology 37 (1), 18–26.

Lenhart, J., Cabaniss, S., MacCarthy, P., Honeyman, B., 2000. Uranium (VI) complexation with citric, humic and fulvic acids. Radiochimica Acta 88 (6), 345.

Lesher, E. K., 2011. Development and application of flow field-flow fractionation - inductively

coupled plasma - mass spectrometry for analysis of uranium speciation and transport in the presence of nanoparticulate ligands. Ph.d., Colorado School of Mines.

Lesher, E. K., Ranville, J. F., Honeyman, B. D., 2009. Analysis of pH dependent Uranium(VI) sorption to nanoparticulate hematite by flow Field-Flow fractionation - inductively coupled plasma mass spectrometry. Environmental Science & Technology 43 (14), 5403–5409.
URL http://dx.doi.org/10.1021/es900592r

Loveland, J., Ryan, J., Amy, G., Harvey, R., 1996. The reversibility of virus attachment to mineral surfaces. Colloids and Surfaces A: Physicochemical and Engineering Aspects 107, 205–221.

Matijevic, E., Scheiner, P., 1978. Ferric hydrous oxide sols: III. preparation of uniform particles by hydrolysis of fe (III)-chloride,-nitrate, and-perchlorate solutions. Journal of Colloid and Interface Science 63 (3), 509–524.

Mibus, J., Sachs, S., Pfingsten, W., Nebelung, C., Bernhard, G., 2007. Migration of uranium(IV)/(VI) in the presence of humic acids in quartz sand: A laboratory column study. Journal of Contaminant Hydrology 89 (3-4), 199–217.

Moulin, V., 2005. Complexation of radionuclides with humic substances. In: Use of Humic Substances to Remediate Polluted Environments: From Theory to Practice. pp. 155–173.
URL http://dx.doi.org/10.1007/1-4020-3252-8_7

Moulin, V., Moulin, C., 1995. Fate of actinides in the presence of humic substances under conditions relevant to nuclear waste disposal. Applied geochemistry 10 (5), 573–580.

Murphy, E., Zachara, J., 1995. The role of sorbed humic substances on the distribution of organic and inorganic contaminants in groundwater. Geoderma 67 (1-2), 103–124.

Murphy, R., Lenhart, J., Honeyman, B., 1999. The sorption of thorium (IV) and uranium (VI) to hematite in the presence of natural organic matter. Colloids and Surfaces A: Physicochemical and Engineering Aspects 157 (1-3), 47–62.

Nachtegaal, M., Sparks, D., 2003. Nickel sequestration in a kaolinite-humic acid complex. Environmental Science & Technology 37 (3), 529–534.

Newman, M., 2011. Melanie's thesis. M.s., Colorado School of Mines.

Penners, N., Koopal, L., 1986. Preparation and optical properties of homodisperse haematite hydrosols. Colloids and Surfaces 19 (4), 337–349.

Prat, O., Vercouter, T., Ansoborlo, E., Fichet, P., Perret, P., Kurttio, P., Salonen, L., 2009. Uranium speciation in drinking water from drilled wells in southern finland and its potential links to health effects. Environmental science & technology 43 (10), 3941–3946.

Ranville, J., Hendry, M., Reszat, T., Q.X., Honeyman, B., 2007. Quantifying uranium complexation by groundwater. Journal of Contaminant Hydrology, 233–246.

Rusch, B., Hanna, K., Humbert, B., 2010. Coating of quartz silica with iron oxides: Characterization and surface reactivity of iron coating phases. Colloids and Surfaces A: Physicochemical and Engineering Aspects 353 (2-3), 172–180.

Ryan, J., Harvey, R., Metge, D., Elimelech, M., Navigato, T., Pieper, A., 2002. Field and laboratory investigations of inactivation of viruses (PRD1 and MS2) attached to iron oxide-coated quartz sand. Environmental Science & Technology 36 (11), 2403–2413.

Schimpf, M., Caldwell, K., Giddings, J., 2000. Field Flow Fractionation Handbook. Wiley-IEEE.

Scholl, M., Harvey, R., 1992. Laboratory investigations on the role of sediment surface and groundwater chemistry in transport of bacteria through a contaminated sandy aquifer. Environmental Science & Technology 26 (7), 1410–1417.

Scholl, M., Mills, A., Herman, J., Hornberger, G., 1990. The influence of mineralogy and solution chemistry on the attachment of bacteria to representative aquifer materials. Journal of Contaminant Hydrology 6 (4), 321–336.

Semiao, A., Rossiter, H., Schafer, A., 2010. Impact of organic matter and speciation on the behaviour of uranium in submerged ultrafiltration. Journal of Membrane Science 348 (1-2), 174–180.

Tinnacher, R., 2008. Effects of fulvic acid and extracellular polymeric substances on the mobility of uranium and plutonium in saturated groundwater systems. Ph.D. thesis, Colorado School of Mines, Golden, CO.

Weishaar, J., Aiken, G., Bergamaschi, B., Fram, M., Fujii, R., Mopper, K., 2003. Evaluation of specific ultraviolet absorbance as an indicator of the chemical composition and reactivity of dissolved organic carbon. Environmental Science & Technology 37 (20), 4702–4708.

Worrall, F., Burt, T., Adamson, J., 2004. Can climate change explain increases in doc flux from upland peat catchments? Science of the Total Environment 326 (1), 95–112.

Zachara, J., Resch, C., Smith, S., 1994. Influence of humic substances on Co2+ sorption by a subsurface mineral separate and its mineralogic components. Geochimica et Cosmochimica Acta 58 (2), 553–566.